Putting Molecules in the Picture: Using Correlated Light Microscopy and Soft X-Ray Tomography to Study Cells

Axel Ekman, Jian-Hua Chen, Venera Weinhardt, Myan Do, Gerry McDermott, Mark A. Le Gros, and Carolyn A. Larabell

Contents

A. Ekman · J.-H. Chen · G. McDermott
Department of Anatomy, University of California, San Francisco, CA, USA
e-mail: axel.ekman@ucsf.edu; Jian-Hua.Chen@ucsf.edu; gerry.mcdermott@ucsf.edu

V. Weinhardt
Molecular Biophysics and Integrated Bioimaging, Lawrence Berkeley National Laboratory, Berkeley, CA, USA
e-mail: VWeinhardt@lbl.gov

M. Do
Biomedical Sciences, University of California, San Diego, CA, USA
e-mail: my.do@ucsd.edu

M. A. Le Gros · C. A. Larabell (✉)
Department of Anatomy, University of California, San Francisco, CA, USA

Molecular Biophysics and Integrated Bioimaging, Lawrence Berkeley National Laboratory, Berkeley, CA, USA
e-mail: mark.legros@ucsf.edu; carolyn.larabell@ucsf.edu; calarabell@lbl.gov

E. J. Jaeschke et al. (eds.), *Synchrotron Light Sources and Free-Electron Lasers*,
https://doi.org/10.1007/978-3-030-23201-6_43

Abstract

Transmission soft x-ray microscopy (SXM) is well suited to visualizing and quantifying mesoscale biology, that is to say structures ranging from the size of a typical molecular machine up to an intact cell. In SXM, the specimen is illuminated with "water window" soft x-rays (i.e., photons with energies in the range 284 eV to 543 eV). The degree to which the illumination is absorbed by a subcellular feature depends on its chemical composition. Carbon- and nitrogen-containing biomolecules strongly absorb the illumination, while water is relatively transparent. Similarities and differences in subcellular molecular content generate contrast in SXM images of the specimen without the use of stains. In this chapter, we discuss the basic concepts behind SXM and describe how 2D SXM data is used to calculate a 3D soft x-ray tomographic (SXT) reconstruction of the specimen. SXT offers significant advantages over other high-resolution cell imaging methods. A particular strength is the capacity to image intact, fully hydrated cells, including eukaryotes such as yeast or mammalian cells. In addition to stand-alone use, we will show that SXT data can be integrated into other imaging modalities to create a comprehensive view of the specimen. The combination of SXT with fluorescence data measured from the same specimen is particularly important, since this allows molecular localization data to be viewed directly in the context of the cell.

Keywords

Cell structure · Chromosome · Correlative imaging · Cryogenic fluorescence tomography · Modeling · Molecular localization · Nucleus · Soft x-ray tomography

Glossary

CCD	Charge-coupled device
CFT	Confocal fluorescence tomography
CFT-SXT	Correlated confocal fluorescence and soft x-ray tomographies
CLEM	Correlated light and electron microscopy
CLM	Cryogenic light microscope
CXDI	Coherent x-ray diffraction imaging
EM	Electron microscopy
FOV	Field of view
FZP	Fresnel zone plate

KZP	Condenser (or Kondenser) zone plate
LAC	Linear absorption coefficient
MZP	Micro (objective) zone plate
NA	Numerical aperture
PSF	Point spread function
SIM	Structured illumination microscopy
SXM	Soft x-ray microscopy
SXT	Soft x-ray tomography
STORM	Stochastic optical reconstruction microscopy
3D	Three-dimensional
WOTF	Weak-object transfer function

Introduction

Imaging is fundamental to our understanding of cell biology. Microscopes capture and present the complexity of a cell in an easy-to-interpret form. For example, a child with a toy microscope can recognize instantly that pond water contains many different types of cell. While this may seem a simplistic example, imagine what it would take to classifying the same sample of pond life by other methods (Megason and Fraser 2007). In the absence of imaging tools, characterizing pond life would require scientific training and access to sophisticated instruments. Given the power of imaging, it should come as no surprise that the development of new imaging methods often results in discoveries, either by producing novel insights or by allowing existing knowledge to be reinterpreted from a new perspective.

Until recently, imaging cells has been the forte of light- and electron-based methods (Subramaniam 2005), with each modality filling a specific niche of specimen size and spatial resolution (see Fig. 1). While these two families of

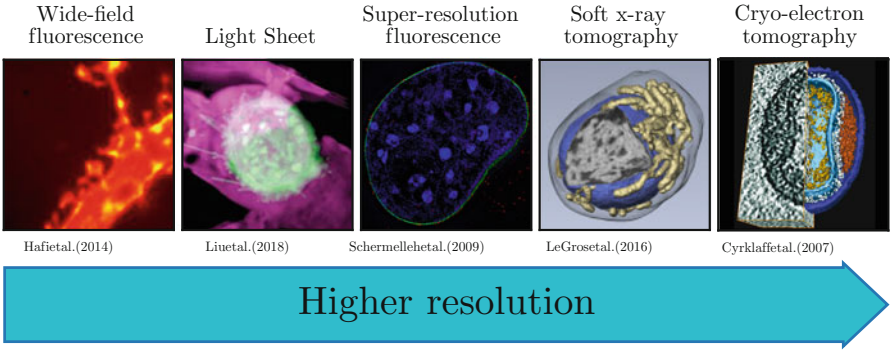

Fig. 1 Comparison of the techniques used to image biological cells. Soft x-ray tomography and super-resolution fluorescence microscopy are in a sweet spot between the low-resolution/large specimen size of wide-field fluorescence microscopy and the high-resolution/small specimen size of electron tomography

imaging tools can cover much of the imaging required, either individually or in combination, they can't completely cover all of the imaging needs in cell biology. For example, electron-based methods are limited to specimens no thicker than 500 nm (Leis et al. 2009). As a result, most cells must be cut into thin sections *prior* to being imaged, making imaging of an entire cell using electron microscopy is a daunting task. Fluorescence microscopy can, of course, image intact cells, even the largest of eukaryotic cells. But, it only produces information on the location of labeled molecules (Giepmans 2006). In fluorescence microscopy, the cellular environment surrounding a localized molecule is left dark, analogous to looking to a distant city at night and seeing lights but not the buildings themselves. So, for some years, there has been effort put toward developing microscopes that can address these shortfalls. Clearly, the obvious solution was to develop microscopes that use an illumination source with characteristics different to light or electrons. Soft x-rays proved to be the answer.

Soft x-ray-based microscopes overcome the thickness constraint imposed by the use of electrons and generate detailed information on the subcellular structure missing from fluorescence images (Larabell and Nugent 2010; McDermott et al. 2012b). However, the application of soft x-rays to cell biology wasn't an overnight success story. Soft x-ray microscopy looked like a promising biological imaging tool for decades, but a number of technical challenges prevented this promise being realized, at least with a reasonable throughput of specimens (Le Gros et al. 2009). Below we describe SXM and the advances that allow cells to be imaged rapidly and in large numbers. We will also cover the methods used to generate quantitative, high-resolution soft x-ray tomographic (SXT) reconstructions from a series of 2D SXM projection images, including representative recent work published using this technique. Finally, we will discuss the combination of structural information derived from soft x-ray tomography combined with molecular localization data produced by fluorescence microscopy. The imaging is done on the same specimen, allowing direct correlation of the two modalities. Molecular location is viewed directly in the context of a reconstructed cell, an exciting advance and a new tool for discovery in cell biology.

Soft X-Rays in Biology

Soft x-rays have long been poorly represented in comparison to hard x-rays in biological research and clinical medicine. Hard x-rays (i.e., x-ray photons with energies greater than 1 keV) are ubiquitous in clinical diagnosis. To the point, most people have a clinical or dental x-ray at least ones in their life. In biological research, hard x-rays have been enormously successful in the form of macromolecular crystallography, a field devoted to determining the atomic structure of crystallized biomolecules. In terms of imaging cells, hard x-rays have yet to make a significant impact. That said, coherent x-ray diffraction imaging (CXDI) and associated methods such as ptychographic imaging have been promoted as having promise in this area. CXDI methods rely on the diffraction, or scattering of x-rays (Holler et al. 2014; Miao et al. 2003). Computer algorithms take the

place of the lenses in a conventional microscope, and the detector camera collects diffraction information from the specimen in reciprocal space, rather than from a real-space projection image. Diffraction patterns are arrangements of intensities that do not resemble the original sample. Obtaining a "real-space" reconstruction of the specimen requires extraction of phase information from measured intensities and calculation of electron density maps (Falcone et al. 2011). The potential to achieve near-atomic resolution in the absence of lens aberrations is certainly an advantage of diffraction microscopy, but this technique still poses many difficulties for imaging cells. The diffraction of noncrystalline specimens, e.g., cells, yields much weaker and diffuse scattering patterns as compared to crystalline structures (Falcone et al. 2011). Samples must also be carefully isolated so that no materials outside of the defined sample boundary contribute to the diffraction pattern, and poor quality or noisy data can render the algorithm ineffective (Chapman et al. 2006). Despite the prospect of very high-resolution imaging and a few exemplary imaging of cells (Shapiro et al. 2005; Huang et al. 2009), hard x-rays have yet to prove their real worth as the basis for new mesoscale imaging tool, which, of course, brings us back to ask, why are soft x-rays so well suited to imaging cells?

The simplest answer, of course, is the highly favorable interaction of soft x-ray photons with biological materials. In combination with recent developments of high-resolution lenses and microscopes operating at cryogenic temperatures, cells can endure larger radiation doses while being imaged in their native state. Soft x-ray photons at "water window" energies (284 eV to 543 eV; 2.34 nm to 4.4 nm) can penetrate intact cells, even large mammalian cells, in their in vivo state of hydration (Attwood 2007; Larabell and Le Gros 2004; Weiß et al. 2000). Moreover, the interaction of water window photons with biological material in cells generates images with excellent contrast (Larabell and Nugent 2010).

Contrast in SXT is derived from differences in density and biochemical composition between the various structures inside the cell. Regions dense in biomolecules strongly attenuate the specimen illumination, whereas high water content areas are much less absorbing (McDermott et al. 2012a). Most importantly, this means that the specimen is imaged directly, with neither the requirement to stain (with heavy metals) nor a priori information (e.g., phase information/clear substrate/etc.).

Soft x-ray illumination operates at much shorter wavelengths than visible light and is therefore capable of imaging a cell at much higher spatial resolution. In summary, soft x-rays offer the opportunity to image a cell in its functional condition and do so quantitatively in 3D with high spatial resolution. Soft x-ray imaging is both unique and highly complementary to other high-resolution structural imaging techniques such as electron microscopy. Consequently, there is a growing availability of soft x-ray microscopes at synchrotron facilities and an even more rapidly expanding community of biologists using soft x-ray imaging to understand structure and function of a cell.

Soft X-Ray Microscopy

Transmission soft x-ray microscopes follow the optical design of a bright-field light microscope (Falcone et al. 2011) with a condenser lens focusing the illumination onto the specimen and an objective transmitting a magnified image of the specimen onto a detector. Refractive indices of x-rays are very close to unity, making the use of traditional visible light optics impractical. Instead, soft x-ray microscopes use optics based on diffraction (Fresnel zone plates) or reflection (capillary) as condensers and objectives. Depending on the microscope design, capillary or condenser zone plate, usually referred to as the KZP to reflect the original German nomenclature, functions as the condenser lens. The objective zone plate is generally known as the micro zone plate (MZP) (Kirz et al. 1995). The soft x-ray illumination adheres to the Beer-Lambert law when it interacts with a biological specimen (Attwood 2007). Attenuation of the illumination by the specimen is, therefore, a linear function of specimen thickness and chemical composition. In addition, using illumination in this region of the spectrum results in an order of magnitude weaker attenuation of photons by water in comparison to carbon (see Fig. 2) (McDermott et al. 2012a). The differential attenuation of soft x-rays results in high-contrast images of cells without the need for chemical fixation or the use of contrast-enhancing staining agents (McDermott et al. 2012a). As a result, cells are imaged in a near-native state.

Assuming correct specimen handling, the quality of the images produced in soft x-rays is determined by the microscope characteristics. High-resolution, high-fidelity imaging requires the specimen to remain stable during data acquisition;

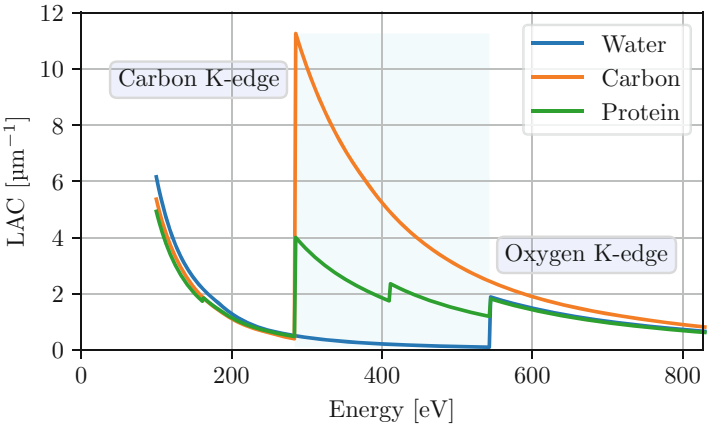

Fig. 2 Plot of photon energy vs. the linear absorption coefficient for carbon (orange), water (blue), and a model protein (green), $C_{94}H_{139}N_{24}O_{31}$. The "water window" region is highlighted in light blue. In this region of the spectrum, water is significantly less attenuating than carbon- and nitrogen-containing biomolecules. The LAC of the model protein also show the nitrogen K-edge at 409.9 eV. (Data from Henke et al. 1993)

any movement during image acquisition causes blurring and loss of resolution and fidelity. The incredibly bright soft x-rays produced by a synchrotron allow images to be collected using short exposure times, in the range of 100 ms to 500 ms. Such short time for image acquisition is of great advantage as it reduces requirement on stability of a specimen, due to such factors as thermal drift in the microscope or specimen stage.

Illumination Sources

Synchrotron soft x-rays are generated by accelerated charged particles, for example, electrons (Attwood 2007) typically confined in a circular orbit. Bunches of electrons – moving at nearly the speed of light – are deflected by a magnetic field, causing a change of the electrons' momentum, which in turn results in the production of electromagnetic radiation in a direction tangential to the initial path. Typically, the electron bunches are deflected by an insertion device in the synchrotron lattice, for example, a bending magnet, wiggler, or undulator. Any type of these insertion devices can, in principle, function as effective illumination sources for soft x-ray microscopes (Rehbein et al. 2009; Le Gros et al. 2014). A full description of the characteristics of insertion devices is clearly beyond the scope of this chapter. However, it should be pointed out that for most SXT data collection, the type of insertion device makes little to no practical difference. For the interested reader, a good description of synchrotron radiation is given by Kim (1989).

While the synchrotron radiation is favorable due to short exposure time, the access to such facilities is rather limited. Hence, a lot of effort has been put in the development of tabletop sources. Currently, the exposure time with laboratory soft x-ray microscopes can be as short as 10 s (Fogelqvist et al. 2017). With potential commercialization of soft x-ray microscopes, 3D imaging of cells in their native state can become available side-by-side with light microscopes in any laboratory.

Optics

In visible light microscopy, the refractive index of glass in the optical elements changes the light path, focusing illumination onto the specimen and transmitting a magnified image of the specimen to the eyepiece or camera. However, in the soft x-ray regime, materials, for example, glass, have a refractive index close to unity (Attwood 2007). Consequently, alternative optical systems to those used in a light microscope are typically employed. Currently, soft x-ray microscopes use Fresnel zone plates and/or a capillary condenser with advanced capabilities to focus x-rays onto the specimen, i.e., function as a condenser (Fig. 3). Fresnel zone plates (FZPs) are nanofabricated pattern of periodic transparent and opaque concentric rings in which the frequency of rings increases toward the outer zone (larger radius) (Attwood 2007; Attwood et al. 2006; Chao et al. 2009; Denbeaux et al. 2001, 2003;

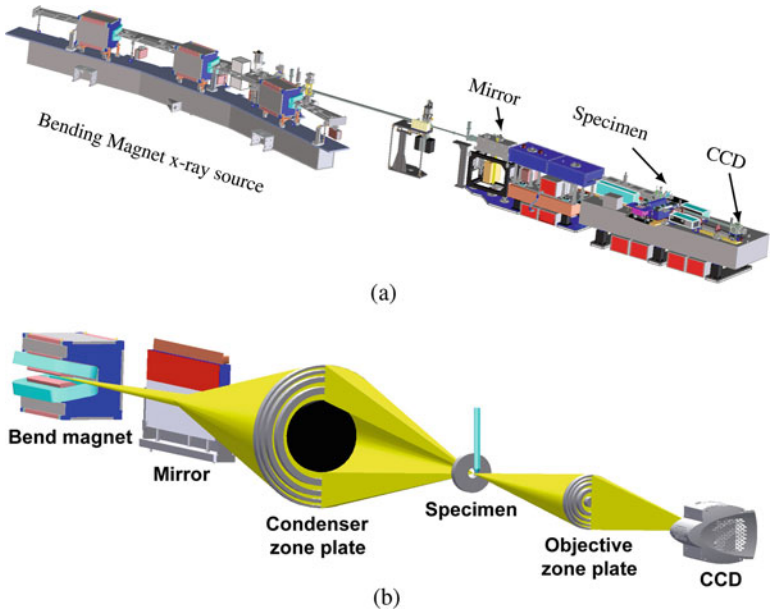

Fig. 3 Optical layouts of soft x-ray microscopes. (a) A schematic showing the overall layout of the microscope XM2 at the Advanced Light Source, Berkeley (b) Illuminating photons from the bending magnet source are directed onto the condenser (a Fresnel zone plate) by a flat mirror. The condenser focuses illumination through an order-sorting pinhole and onto the specimen. The objective (another Fresnel zone plate) focuses transmitted illumination onto the CCD detector. Microscopes equipped with a capillary condenser eliminate the need for the order-sorting pinhole but require some type of monochromator upstream in the optical path

Schneider et al. 2003). Due to the transparent/opaque structure of FZPs, the incident x-rays constructively interfere at the focal point. Alternatively, a capillary condenser can be used to focus the soft x-ray illumination onto the specimen (Schneider et al. 2012). Capillary condensers take advantage of the grazing incident reflection of x-rays on the inner surface of the capillary, either as a single "bounce" or by guided multiple reflections. Irrespective of whether the microscope is equipped with a capillary or a zone plate condenser, the condenser produces a spot of light with a tight focus, typically smaller than most specimens. The condenser must, therefore, be rapidly scanned or shaken during data acquisition to create uniform illumination across the field of view.

Image Formation

Since transmission soft x-ray microscopes are conceptually similar to a simple bright-field light microscopes, they share the same physical limitations on the resolution and depth of field. A key assumption has traditionally been that the soft

x-ray microscopic images can be regarded as images of classical projections, if the depth of field encloses the sample (Haddad et al. 1994; Weiß et al. 2000). This means that the resolution, limited by that of the optical system, $r \propto \lambda/NA$, also imposes a size limit on the specimen $L \propto \lambda/(NA)^2$ for full-rotation tomography and to $L \propto \lambda \left[\sin\theta(NA)^2\right]$, for limited-tilt imaging, where θ is the maximum tilt angle of the measurement, λ is the wavelength of the illumination, and NA is the numerical aperture of the objective lens. Extending the capabilities of the microscope beyond these assumptions requires a proper modeling of the image formation.

In tomography, the model of image formation has been traditionally based on the Radon transform (Radon 1917), which is the ideal linear transform (projection) of the specimens' attenuation coefficients onto a plane. This is linked to the experimental image formation through the Beer-Lambert law, such that the recorded intensity of a ray, I_i, can be expressed as attenuation of its intensity along a ray-path, L_i, such that

$$I_i = I_{i0} \exp\left[-\int_{L_i} \mu_{L_i}(t)\,\mathrm{d}t\right], \tag{1}$$

where $\mu_{L_i}(t)$ is the linear absorption coefficient (LAC) of the specimen along the ray-path and I_{i0} the unattenuated intensity incoming onto the specimen. There are two approximations related to this kind of ideal image formation. Firstly, it assumes that the wave propagation through the sample is diffraction free and the intensity after the sample can be calculated by parallel beams adhering to the Beer-Lambert law. Secondly, it assumes that the recorded intensity of the image is directly proportional to the intensity of the field at the vicinity of the sample.

A proper inclusion of the wave propagation in the image formation involves solving the Helmholtz equation in the sample space. As to date, this has only been done for the forward model, both in 2D (von Hofsten et al. 2007; Bertilson et al. 2011a) and 3D (Selin et al. 2014). A general way to integrate this into the inverse problem, i.e., the reconstruction scheme, however, remains elusive.

The assumption that the recorded image is linear with intensity requires a perfectly incoherent image formation with no blurring of the point spread function (PSF). In general SXM behaves in a partially coherent system in which the (spatial) partial coherence can be expressed by the ratio of the numerical apertures:

$$m = \frac{NA_c}{NA_o}, \tag{2}$$

of the incoming light from the condenser, NA_c and collected light by the objective, NA_o. For $m \to 0$, the imaging behaves coherently (i.e., a linear transform of the field), and for $m \to \infty$, the imaging is fully incoherent (linear transform of the field intensity). In all other cases, the system is partially coherent. Partial coherence is known to have an effect on the recorded image (Jochum and Meyer-Ilse 1995; Sheppard 2004), but a general backward model for this bilinear transform (Hopkins 1953) is yet to be presented. Within the assumption of a valid weak-object transfer

function (WOTF) (Streibl 1985; Sheppard and Mao 1989), partial coherence can be included in the reconstruction (Knöchel 2005) but is limited to the Born approximation (Slaney et al. 1984; Trattner et al. 2009).

When the approximation of both diffraction-free propagation and incoherence (linear intensity transform) is valid, (Otón et al. 2012) provide a solution, requiring that the PSF of the optical system encloses the whole sample. In this case, the ideal Beer-Lambert projections can be obtained by deconvolution of the projection images. This model coincides with the assumption of parallel projections when the PSF is narrow (a delta function).

In cases where the imaging is limited by the depth of field, it can be effectively extended by focus stacking in either projection space (Liu et al. 2012; Otón et al. 2017) or reconstruction space (Li et al. 2017) or integrated into the reconstruction scheme (Klukowska et al. 2014; Selin et al. 2015). Recent results from a linear approximation of the model of Otón et al. (2012) have also included the image formation model directly into the reconstruction scheme, improving thus the quality of the tomographic reconstructions (Ekman et al. 2018).

Instrument Locations and Current Status

SXT is a relatively new modality for imaging cells, at least compared to electron or light microscopy. The first report of successful SXT being carried out on an individual cell only dates back to Weiß et al. (2000). While this might seem an eon ago, in terms of synchrotron-based experiments – where it can easily take a decade to fund, design, and build a novel instrument – this is the typical pace at which new technologies evolve.

Currently, there are two designs of soft x-ray microscope in operation at synchrotron facilities across the world (see Table 1). Most of them use a single-bounce capillary as the condenser and a sample stage adopted from electron microscopy.

The soft x-ray microscope at XM2, located at the Advanced Light Source in Berkeley, USA, is the only microscope where KZP serves as a condenser and sample

Table 1 Soft x-ray microscopes in operation and development

Microscope	Research facility	Location	Reference
U41-TXM	BESSY II	Berlin, Germany	Schneider et al. (2010, 2012)
XM2	ALS	Berkeley, USA	Parkinson et al. (2013) and Le Gros et al. (2014)
MISTRAL	ALBA	Barcelona, Spain	Pereiro et al. (2009) and Sorrentino et al. (2015)
B24-TXM	Diamond	Didcot, UK	Harkiolaki et al. (2018)
BL07W	NSRL	Hefei, China	Guo et al. (2017) and Liu et al. (2018a)
24A	NSRRC	Hsinchu, Taiwan[a]	(Su et al. 2016)

[a]The microscope at NSRRC is still in the development phase

is mounted on the custom-designed sample stage. XM2 was designed, built, and now operated by the National Center for X-ray Tomography (NCXT; http://ncxt.lbl.gov/). In terms of the exact imaging characteristics, it is sufficient to say that both are equally well suited to imaging cells.

Since the development of plasma sources in the early 1980s (e.g., Michette et al. 1993 and references therein), there has been a steady improvement in tabletop imaging (Rymell and Hertz 1993; Berglund et al. 2000; Horne et al. 2009; Bertilson et al. 2009, 2011b; Hertz et al. 2012). Sub-50 nm resolution has been readily achieved, but the necessary exposure times still range from 30 s (Carlson et al. 2013) to a minute or two (Kim et al. 2006; Hertz et al. 2012), which is at least an order of magnitude higher than what is commonly used at synchrotron facilities. Nevertheless, commercial devices are beginning to emerge, such as Excillum,[1] SIRIUS XT[2], and Energetiq,[3] providing laboratory-scale solutions to the SXT illumination, and recent progress has pushed the exposure time as low as 10 s (Fogelqvist et al. 2017) with a 100 nm 3D resolution.

Soft X-Ray Tomography

Tomography is the process of calculating a 3D reconstruction of the specimen using a series of 2D projection images collected sequentially around a rotation axis (Natterer 1986). For biological specimens, such as cells, repeated exposure to harsh x-ray illumination results in cumulative radiation damage, unless the specimen is either chemically fixed or held at cryogenic temperatures. Chemical fixation is easily achieved by treating the specimen with cross-linking aldehydes. However, this method has been shown to cause irreversible damage to the ultrastructure of the cell regardless of the measures taken to avoid it (Lučić et al. 2007). So, mitigation of radiation damage during image acquisition is preferentially achieved by plunging the specimen into liquid propane cooled by liquid nitrogen (McDermott et al. 2012a) or by rapid cryo-cooling in a high-pressure freezing device of the type developed and used routinely by the electron microscopy community (Weiner et al. 2013).

SXT data are acquired in microscopes fitted with FZP objectives that produce a spatial resolution in the 25 nm to 50 nm range (Falcone et al. 2011). During data acquisition, the soft x-ray beam diffracts around the opaque rings to a focal point. The spacing in the outermost Fresnel zone determines the maximum spatial resolution achievable. While zone plates offering spatial resolutions better than 25 nm have become available (Chao et al. 2005, 2009), they are not yet in common use for several reasons. Use of higher-resolution plates results in a depth of focus shallower than the thickness of the specimen (McDermott et al. 2012b), thereby

[1] https://www.excillum.com/

[2] https://siriusxt.com/

[3] https://www.energetiq.com/

requiring the collection of several through-focus images at each angular position. This process not only increases the x-ray dose on the specimen; it adds significant additional complexity to data processing and analysis.

As with any imaging experiments, soft x-ray microscopy begins with preparation of the specimen. Any artifacts introduced as a result of poor specimen preparation persist throughout data acquisition to the final reconstruction and potentially result in confusing or misleading information. Fortunately, specimens require minimal preparation before being imaged by SXT (Parkinson et al. 2013). Cells are simply transferred from their growth environment into a specimen holder and immediately cryopreserved. The total time required for this procedure is short, typically less than a minute. Consequently, cells imaged by SXT are maintained very close to their native state, which is to say, not only intact and fully hydrated but never exposed to harsh chemical fixatives or heavy metal stains. Minimal specimen preparation is one of the highlights of the SXT. We will now briefly outline the steps required for SXT.

Specimen Mounting

To impart mechanical stability and allow rotation during tomographic data acquisition, cells must be mounted in a specimen holder (Parkinson et al. 2013). The holder can take many forms, as long as the design can withstand both the incoming radiation and the low temperatures for extended periods and be robust enough to handle and easy to manipulate. Currently, two specimen holders are in common use for SXT: grids and capillaries (see Fig. 4). Each has advantages and disadvantages, but the choice of specimen holder comes down to cell size and the type of cryo-rotation stage installed in the microscope.

Flat-Grid Specimen Mounting

Flat grids used in SXT are similar, if not identical, to those used for electron microscopy (EM) (Carzaniga et al. 2014). Consequently, this design of specimen holder is optimal when the microscope is equipped with a modified EM cryo-rotation stage. This stage design is also best suited to imaging large (laterally extended) specimens (Carzaniga et al. 2014; Schneider et al. 2012), and cells can be cultured directly on the holder surface. The drawback is the limitations placed on grid tilt (rotation) during SXT data acquisition (Smith et al. 2014a; Cinquin et al. 2014). As the grid is tilted to higher angles, the specimen thickness progressively increases to the point of illumination being fully absorbed. The limit on grid rotation, usually −70° to 70°, leads to a "missing wedge" of data that impacts the fidelity of the tomographic reconstruction of a specimen. Moreover, depending on the resolution of the zone plate used, cell structures above and below the focal plane will be out of focus. Even so, grids can produce high-quality images and reconstructions of well-chosen specimens.

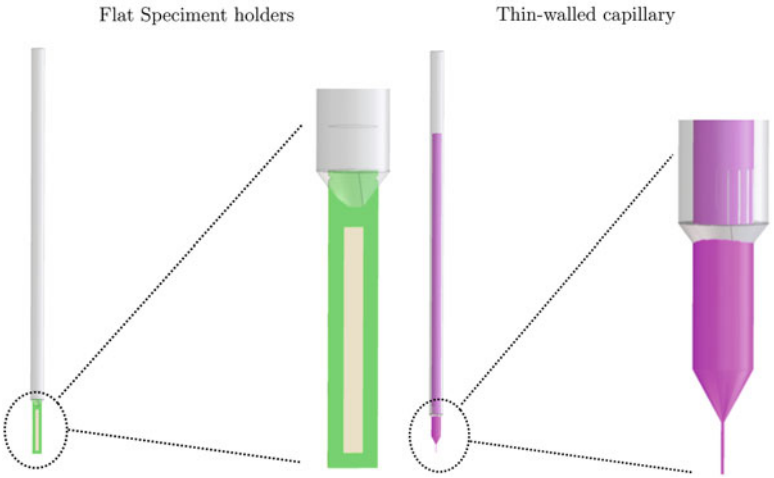

Fig. 4 The two types of specimen holder commonly used in soft x-ray microscopes. (Left) Flat grids are similar to those used for EM and are suitable for imaging of large (flat) cells. Increased size capacity of the holder comes, however, with a drawback, as the limitation on the rotation leads to a "missing wedge" of data from certain angles of the sample. (Right) Thin-walled capillaries allow for full 360° rotation of the sample but put restrictions on the sample size, as the whole sample has to be confided in a cylinder

Capillary Specimen Mounting

Thin-walled glass capillaries can also be used as specimen holders for SXT (McDermott et al. 2012b). The capillaries are made by heating and pulling a glass capillary such that the tip (the "observation area") has a diameter of 4 µm to 16 µm and a length of ∼300 µm (Gros et al. 2012) (see Fig. 4). Cells must be within this observation area to ensure that the soft x-ray beam can penetrate the specimen, and it is in the field of view of the CCD camera. Capillary specimen mounting enables full angular rotation and thus the capture of valuable information at higher rotation angles. This mounting method is particularly suitable for non-adherent cells, such as red blood cells or lymphocytes, and smaller samples, such as yeast or bacteria (Carzaniga et al. 2014). Capillary mounting is also a good choice when imaging tissues, such as those from mouse models, since the dissociated cells maintain the shape normally found in the body (Clowney et al. 2012). Most cells can be loaded directly into the capillary via pipetting *prior* to cryo-fixation and imaging (Gros et al. 2012; Parkinson et al. 2013). Cells with average diameters greater than 12 µm or those suspended in viscous solutions, e.g., containing matrix proteins, require gentle external force to either pull (via centrifuge) or push (via external syringe pump) the cells into the tapered observation area of the capillary.

Cryopreservation

To mitigate specimen degradation during imaging, a biological specimen must be "fixed," either chemically or cryogenically, prior to SXT data acquisition. Chemically fixing cells is a straightforward process; the cells are simply placed in a solution containing aldehydes, typically paraformaldehyde and/or glutaraldehyde. The aldehydes form covalent bonds between proteins in the cell. Unfortunately chemical fixation is far from ideal in terms of SXT. Firstly, the cross-linking of proteins causes disruption of the native cell structures in an unpredictable manner, with aldehydes causing potentially devastating changes to the subcellular organization (Lučić et al. 2007), including a significant decrease in cell volume after fixation (Hanssen et al. 2012). Secondly, the aldehyde adds carbon content to the cell in a non-specific manner. Subsequent SXT reconstructions would not just include attenuation of the illumination by the specimen alone but the combination of specimen and unknown amounts of fixative.

Cryopreservation has, on the other hand, been shown, using high-resolution electron microscopy (EM), to retain delicate, fine structural details typically destroyed by chemical fixation (Dubochet et al. 1988; Dahl and Staehelin 1989). Cryopreservation of cells for SXT is merely a case of cooling the mounted specimen faster than structure-destroying crystalline ice can form. In cryo-EM, where the spatial resolution is significantly higher, this step can be problematic; even the growth of minuscule crystals will be apparent in images. However, the lower resolution of SXT means any cryopreservation artifacts, at this size scale, are not visible in images. In the future – as SXT at higher spatial resolutions becomes the norm – methods such as high-pressure freezing may emerge as the preferred cryopreservation method (Weiner et al. 2013).

Data Acquisition

Irrespective of the soft x-ray microscope design, SXT data can be acquired very rapidly, with exposure times for each projection image in the millisecond to second regime. Automated cryogenic goniometer stages rotate the specimen according to a predetermined data collection strategy. For capillary-mounted specimens, this means recording projection images typically over 180° or 360°. When the cells are mounted on a grid, the total angular displacement is limited by the sample stage and varies between 100° to 140° (Cinquin et al. 2014). In either case a single field of view tomographic data set can be collected in a few minutes. Since the specimen holders contain multiple, potentially interesting fields of view (FOV), each holder typically yields a number of tomographic data sets. Each FOV can accommodate a single mammalian cell or a large number of bacterial or fungal cells. In the case of bacteria mounted in a capillary, a single FOV can contain upward of 50 cells (McDermott et al. 2012b). Consequently, in less than an hour, it is possible to obtain sufficient data to reconstruct several hundreds of bacterial cells or, in the case of larger cells, such as yeast, tens of cells.

Reconstruction

Tomographic reconstruction is the process of using aligned 2D images collected from different angles to calculate a 3D representation of the specimen (Natterer 1986). In an idealized experiment, the series would contain an infinite number of noiseless, perfectly aligned images. In this scenario the choice of reconstruction algorithm would be moot, since all competent algorithms would generate the same reconstruction. However, real-world acquisitions contain a finite number of images and both noise and imperfections in their alignment (Parkinson et al. 2012). The choice of the best algorithm to use for the reconstruction of a given data set is often a matter of trial and error.

As SXT acquisition time is limited by the radiation dose which a sample can withstand, the data sets are often limited by a low number of projections and/or low signal-to-noise ratio of the images. Furthermore, many microscopes operate with limited stage mobility, resulting in a "missing wedge" of projection data. This means that direct reconstruction methods perform, in general, quite poorly. There are various ways to overcome the instabilities of the direct inversion, which in practice leads to a vast pool of reconstruction methods or algorithms. Iterative methods provide robust ways to solve even highly noisy or undersampled data sets. These algorithms iteratively refine the reconstruction by correcting it based on the measured projection data (Beister et al. 2012). An example of six different reconstruction algorithms on the same data is shown in Fig. 5. The data was taken at NCXT and consists of 83 evenly spaced projections over a range of 180°.

Fortunately, tomography is ubiquitous in a wide range of fields – from materials science and electron tomography to clinical diagnosis. As a result, a significant effort has gone into the development of reconstruction algorithms and methods, resulting in a plethora of readily available software for this task, e.g., AREC3D (Parkinson et al. 2012), ASPIRE (Fessler 1995), ASTRA (van Aarle et al. 2016), bsoft (Heymann and Belnap 2007), IMOD (Kremer et al. 1996), PyHST2 (Mirone et al. 2014), Tomo3D (Agulleiro and Fernandez 2015), and TomoPy (Gürsoy et al. 2014). There are also several reconstruction schemes that have been tailored for SXT data (Selin et al. 2015; Otón et al. 2017; Ekman et al. 2018).

Segmentation

Segmentation is the process of partitioning an image into nonoverlapping regions. In terms of an SXT reconstruction of a cell, this means identifying structures of interest such as whole cells, or individual organelles, in order to isolate a particular component of the data set (Gros et al. 2012; Parkinson et al. 2013). Segmentation simplifies the data representation both from a visualization point of view and enables quantifiable analysis of the organelles in the cell, such as density differences (Uchida et al. 2011; Myllys et al. 2016), spatial distance metrics such as distances between

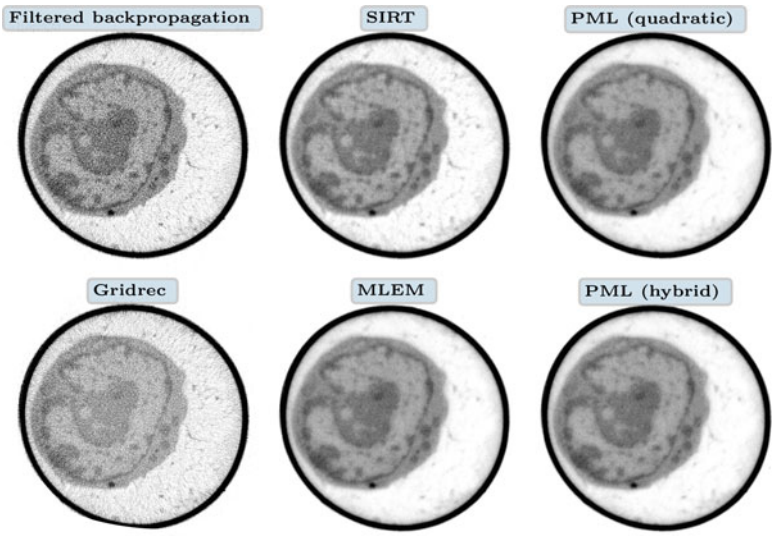

Fig. 5 An example of the effect of different tomographic reconstruction algorithms. The presented reconstruction methods shown here consist of two direct methods, filtered back projection (Bracewell 1956) and Gridrec (Dowd et al. 1999); two unregularized iterative methods, SIRT (Gilbert 1972) and maximum likelihood (Dempster et al. 1977); and two penalized maximum likelihood methods, one with a quadratic penalty (Fessler 1996) and one with a hybrid (linear and quadratic) penalty (Chang et al. 2004). Reconstructions were calculated using TomoPy (Gürsoy et al. 2014)

organelles, and morphometrics (Uchida et al. 2011; Darrow et al. 2016). In SXT, this process is based on the measured linear absorption coefficient (LAC) and guided by structural cues and subcellular location.

As many cellular structures differ in their protein density, the voxel intensity is often an effective parameter to identify boundaries of features and many organelles. For example, nucleus, nucleolus, mitochondria, and lipids can be readily identified from the reconstructed volume (Uchida et al. 2011). Presently, however, image segmentation is a time-consuming, largely manual process (Parkinson et al. 2013), as the detection of these features requires expertise and biological knowledge. This manual segmentation may be assisted by commercially available software such as Amira or Avizo,[4] or specifically designed workbenches (Luengo et al. 2017); however these programs still require significant input from the user. There are also efforts to distribute the manual labor, using crowdsourcing (Good and Su 2013), such as "etch a cell".[5]

[4] FEI Software: https://www.fei.com/software/

[5] https://www.zooniverse.org/projects/h-spiers/etch-a-cell

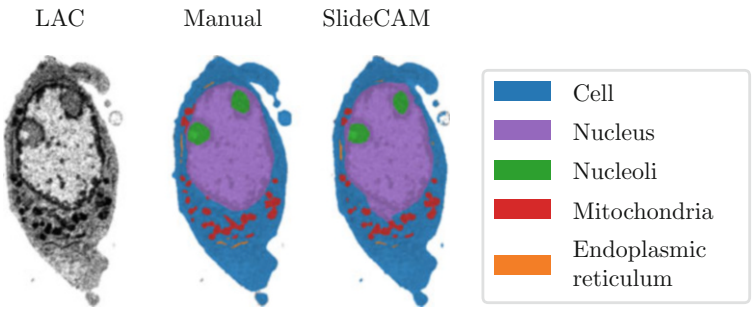

Fig. 6 Example of a trained multi-class labeling using SlideCAM[6] environment to apply the algorithm presented by Pelt and Sethian (2018) on an SXT image of a human T cell

Automatic segmentation of SXT data remains the most desirable, however challenging, way. Over the past years, Convolution Neural Networks (CNNs) have become an area of very active research and have been successfully applied to various segmentation problems (Roth et al. 2014; Ciompi et al. 2015; Shkolyar et al. 2015; Zhang et al. 2015; Çiçek et al. 2016; Pelt and Sethian 2018). One such example is shown in Fig. 6.

Many subcellular features cannot be distinguished on the basis of LAC values alone, as their protein content is similar to their surroundings (such as secretory vesicles or the Golgi apparatus) or because of similar shape (various protein aggregations cannot be distinguished from other organelles with similar density). In these cases, their identities are to be confirmed by correlation with fluorescence imaging (Cinquin et al. 2014; Gros et al. 2012; Parkinson et al. 2013; Smith et al. 2013; McDermott et al. 2012a).

Examples

A number of recently published SXT reconstructions are shown in Figs. 7, 8, 9, and 10. SXT can be applied to a wide range of specimen types, from small bacterial cells to large, extended cells or tissue sections. In all cases the information is generated from specimens that have been maintained true to their in vivo, functional state. It bears repeating one more time that imaging biological specimens at high resolution only makes sense when the specimen is near native state. Otherwise it is akin to imaging beef jerky and drawing highly detailed conclusions about muscle structure in a live cattle. The scientific merit of any tomographic reconstruction is not a function of spatial resolution but primarily dependent on the fidelity of the specimen and the information obtained.

[6] https://slidecam-camera.lbl.gov/

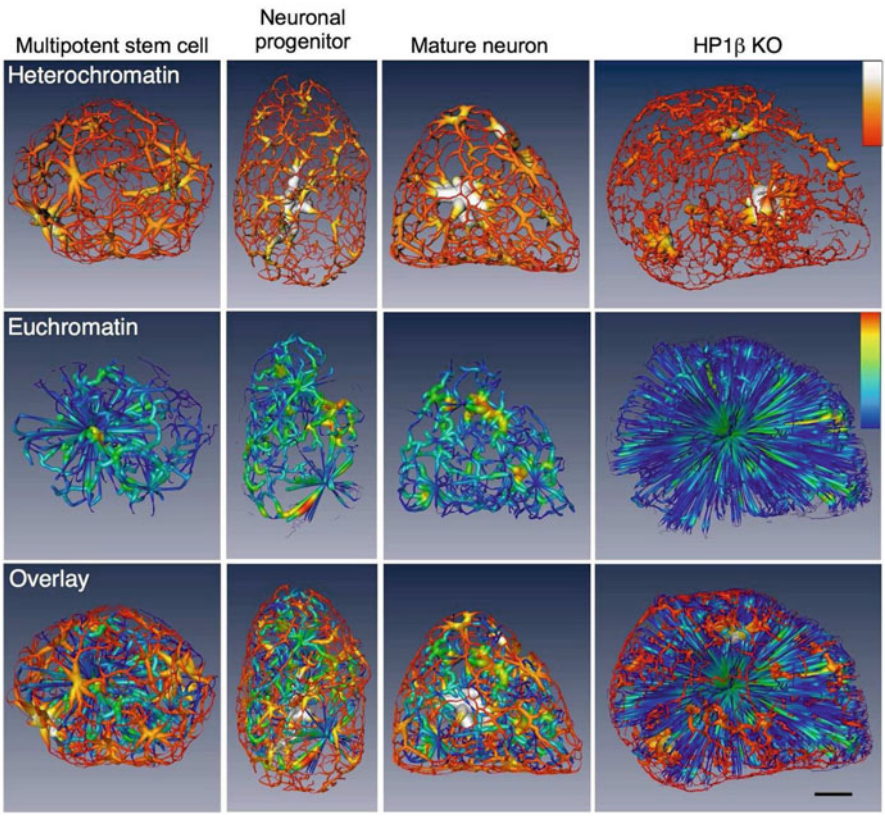

Fig. 7 Soft x-ray analysis of chromatin masses in the nuclei of three types of olfactory epithelium cells, namely, multipotent stem cells, neuronal progenitors, and terminally differentiated neurons, together with similar data from HP1β knockout cells. This morphological study revealed that a surprising degree of connectivity exists between chromatin, which persists throughout development and differentiation. Scale bar = 2 μm. (Taken from Le Gros et al. 2016)

Correlated Light Microscopy

Fluorescence microscopy locates intracellular structures or molecules tagged with fluorescent protein labels (Tsien 2005). A notable disadvantage of this technique is the near-invisibility of the intracellular contents surrounding the fluorescent labels. A way to overcome this disadvantage is to combine fluorescence imaging with a complementary modality that does not suffer from the same disadvantage.

An example of this is correlated light and electron microscopy (CLEM) which has been under development for more than 40 years (Ellisman et al. 2012). While astonishing progress has been made (Kopek et al. 2012), the physical characteristics of EM and the light microscopes used in this work have proved to be limited. In particular, the specimen thickness limit of 500 nm for EM restricts the total

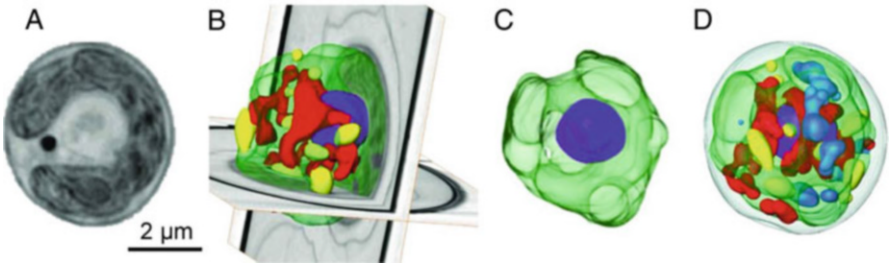

Fig. 8 The morphology of the green algae *C. zofingiensis* imaged by soft x-ray tomography. (**a**) Representative orthoslice of the reconstructed cell. (**b**) Three-dimensional segmentation overlaid with two orthogonal orthoslices. (**c**) Segmented chloroplast and nucleus. (**d**) Fully segmented cell. Color key: nucleus (purple), chloroplast (green), mitochondria (red), lipids (yellow), and starch granules within the chloroplast (blue). (Image from Roth et al. 2017)

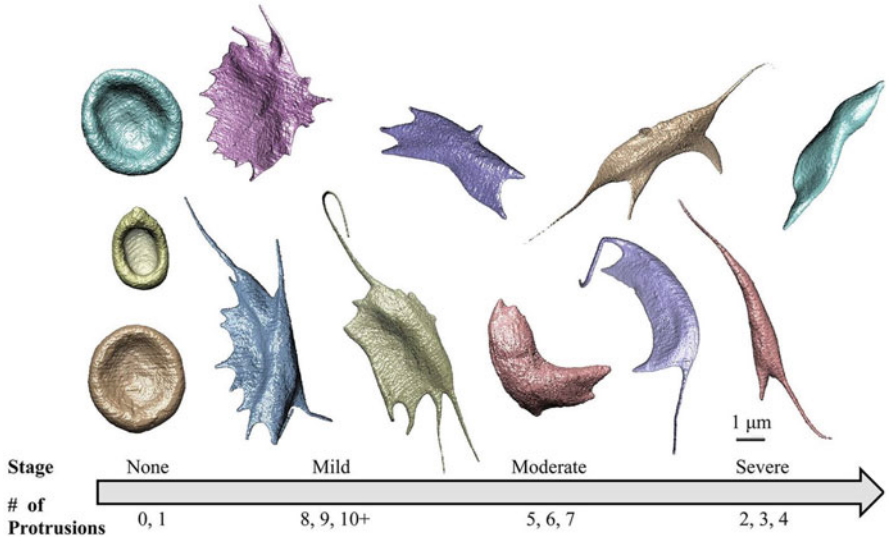

Fig. 9 Morphological study of the four stages of sickle cell anemia in red blood cells carried out by soft x-ray tomography. Following volumetric analysis to correlate protrusion number with density, a hallmark of sickle cell disease, data were binned into four categories. The none category is composed of red blood cells (RBCs) with zero or one protrusion; the mild category is composed of RBCs with eight, nine, ten, or greater protrusions; the moderate category is composed of RBCs with five, six, or seven protrusions; and finally, the severe category is composed of RBCs with two, three, or four protrusions. (From Darrow et al. 2016)

field of view that can be imaged in a reasonable time frame (Leis et al. 2009). Moreover, light microscopes used in most of this work have typically been equipped with low numerical aperture lenses, resulting in relatively low-resolution molecular localization information.

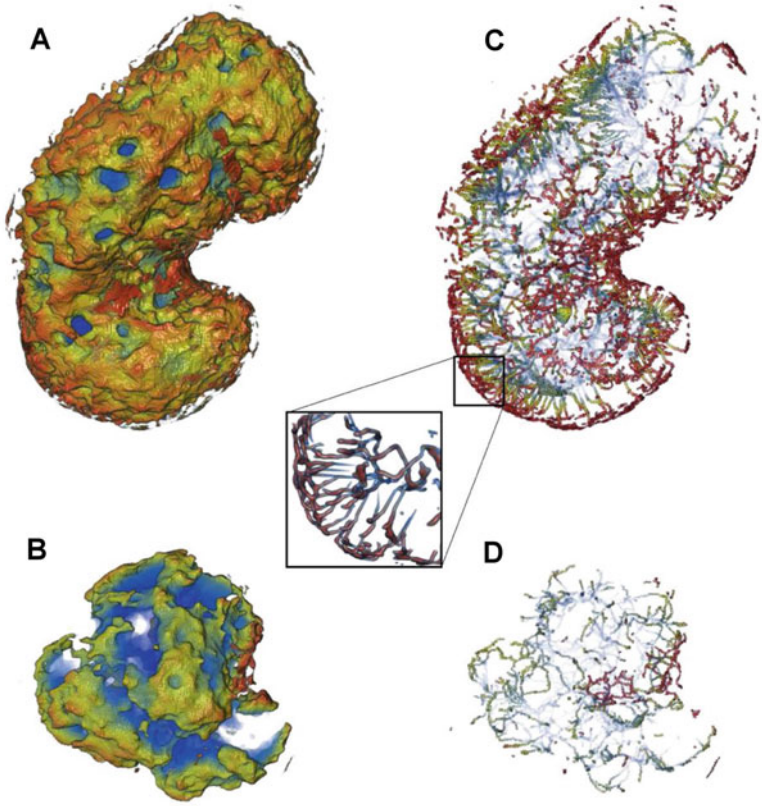

Fig. 10 Soft x-ray tomographic study of the subcellular changes associated with herpes simplex virus infection. Low-LAC regions of the nucleoplasm with (**a**) and without (**b**) viral replication compartments (VRCs) adjacent to the nuclear envelope. A computationally reduced skeletonized structure of the low-LAC regions in the μm-thick layer of host chromatin close to the nuclear envelope, which shows channels across the peripheral heterochromatin in infected (**c**) as well as non-infected (**d**) cells. Pseudo-color indicates (increasing from red to blue) the distance from the nuclear envelope. These results demonstrated that HSV-1 infection induces the formation of channels penetrating the compacted layer of cellular chromatin and allowing for the passage of progeny viruses to the nuclear envelope, their site of nuclear egress. (Image taken from Myllys et al. 2016)

SXT overcomes the specimen thickness constraint, and the development of a high-numerical aperture (NA) confocal cryogenic light microscope (CLM) overcomes the limitation on the spatial resolution with which molecules can be localized (Le Gros et al. 2009; McDermott et al. 2009). This microscope incorporates a custom specimen-imaging compartment that is filled with a cryogenic immersion fluid, typically liquid propane (refractive index = ∼1.33) which is well-matched to the 1.3-NA lens of the CLM (Le Gros et al. 2009). As a result the refractive index mismatch between the specimen and lens is minimized, leading to more

efficient light collection (Le Gros et al. 2009; Smith et al. 2014a). Most importantly the immersion fluid increases the NA of the microscope, thereby increasing the maximum attainable spatial resolution. The resolution for this high-NA CLM is ~250 nm (Le Gros et al. 2009), while that of a standard CLM is 400 nm to 500 nm (Kaufmann et al. 2014b).

This CLM was equipped with a specimen rotation stage, similar to the one used in the soft x-ray microscope, to allow tomographic data collection (cryogenic confocal fluorescence tomography, CFT) (Smith et al. 2013, 2014a; Cinquin et al. 2014). As a result two separate 3D data sets (SXT and CFT) from the same specimen can be calculated and then combined and correlated. Combining data with similar dimensionality and spatial resolution is the optimal correlated imaging experiment (Fig. 11).

Co-alignment

To generate an accurate, faithful representation of the specimen in terms of both types of data, CFT and SXT data must be aligned to each other with high accuracy. The best co-alignment strategies are clearly objective, robust, and highly reproducible. Ideally, positional errors in aligning the two data sets will be considerably less than the resolution of the higher-resolution modality.

In CLEM, these criteria have been met most effectively by using fiducial markers that are visible in both modalities (Giepmans et al. 2005; Hagen et al. 2014; Martone et al. 2000; Schellenberger et al. 2014; Van Rijnsoever et al. 2008; Zeev-Ben-Mordehai et al. 2014). For CFT-SXT fluorescent polystyrene microspheres can be used for this purpose, as can surface-functionalized fluorescent gold nanoparticles

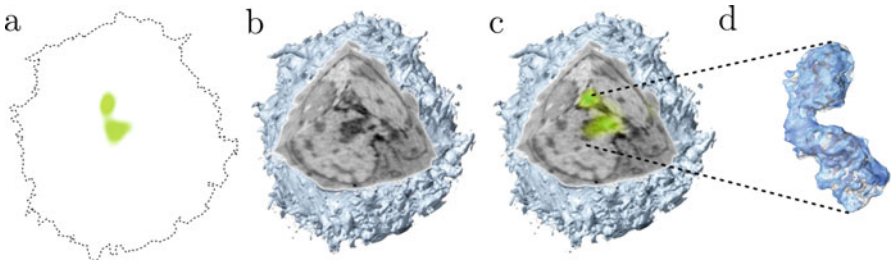

Fig. 11 Correlated CFT-SXT imaging of female v-abl macroH2A-EGFP transformed thymic lymphoma cells. (**a**) A 2D projection of the inactivated X chromosome (Xi) CFT reconstruction. (**b**) Cutaway of a volume-rendered SXT reconstruction. The surface of the cell is colored light blue. LAC values are represented in gray scale, ranging from high (dark) to low (light). (**c**) The CFT reconstruction shown in (a) overlaid into the volume-rendered SXT reconstruction shown in (**b**). (**d**) Surface rendering of Xi segmented from the SXT reconstruction after identification by macroH2A-EGFP CFT. The deep blue-shaded areas are regions of high x-ray linear absorption coefficient (LAC) that make contact with the nuclear envelope. (Image adapted from Smith et al. 2014b)

(Smith et al. 2013, 2014a). The general workflow for a CFT-SXT-correlated imaging study is described in Cinquin et al. (2014).

The 2D image data taken from SXT and CFT, respectively, can be processed independently of one another to generate two separate 3D reconstructions. Though the spatial resolutions of the two techniques are not yet optimally comparable, the information attained from each has been correlated successfully. The 100 nm gold nanoparticles bound to the exterior of the capillary act as fiducial markers for individual alignment of the two tomographic data sets. Due to high electron density and light absorption, gold beads are easily distinguished from their surroundings in CFT and SXT projections (Baev et al. 2002; Smith et al. 2013).

Excluding one fiducial marker from the transform calculation that co-aligns the two reconstructions and predicting the location of that fiducial is a straightforward means of estimating the accuracy of the correlation. Comparison of calculated positions with the actual positions gives an estimate of the error (Cinquin et al. 2014). Repeating these steps for each fiducial across all tomograms in the data set can provide a direct readout of the correlation accuracy (Cinquin et al. 2014; Kukulski et al. 2011). Figure 11 shows a recent result of correlated CFT-SXT imaging.

Toward Super-Resolution

Imaging fluorescent specimens at cryogenic temperature offers many positives over room temperature imaging. Cryogenic temperatures significantly increase the working life of the fluorescent labels, therefore overcoming the issue of signal loss due to the fluorescent label being photo-bleached by the illumination (Le Gros et al. 2009). Irreversible photo-bleaching is also less dependent on the local chemical environment at colder temperatures, making it possible to more accurately quantify the local concentration of a labeled protein.

The development of super-resolution fluorescence techniques pushed the resolution beyond the long-existing diffraction limit and is emerging also for cryo-immobilized specimens (Kaufmann et al. 2014a). Techniques such as structured illumination microscopy (SIM) (Gustafsson 2000; Gustafsson et al. 2008; Schermelleh et al. 2008) also benefit from the increased working life of the fluorescent labels and appear well-suited to being used in tandem with SXT, particularly in terms of spatial resolution.

Combining imaging techniques compensates for the inherent insufficiencies of individual microscopes, thus improving the completeness of experimental data and widening visualization capabilities. There are many available methods (Huang 2010) to choose from in terms of super-resolution. One such example is shown on Fig. 12 where stochastic optical reconstruction microscopy (STORM) was combined *prior* to the vitrification, to obtain similar resolution in both the volumetric image of LAC from SXT and the localization of fluorescent particles.

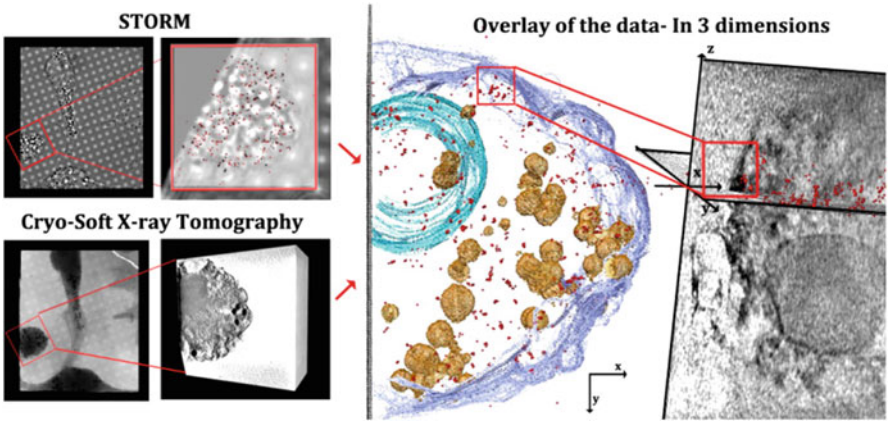

Fig. 12 Correlated cryo-soft x-ray tomography (cryo-SXT) and stochastic optical reconstruction microscopy (STORM) by Varsano et al. (2016), showing co-localization of cholesterol crystals in macrophage-like RAW 264.7 cells. (Image from Varsano et al. 2016)

Summary of Current Capabilities and Future Outlook

SXT and correlated CFT-SXT are exhilarating new additions to the portfolio of biological research tools available at synchrotron light sources. In the future, these modalities will contribute significantly to community-wide efforts aimed at generating cell models that range in scale from atomic to cellular levels.

Soft x-ray tomography is now recognized as a valuable modality for imaging biology. SXT is an effective way to visualize and quantify the subcellular structure of cells maintained in a near-native state. Soft x-ray microscopes are currently capable of generating 3D cellular reconstructions that have a spatial resolution of 35 nm to 50 nm. In the near future, the achievable resolution will increase as higher-resolution zone plates become available. This enhancement will require the development of new data collection strategies and data processing methods that take account of the decreased depth of field (DOF). As usage of high-resolution optics results in a DOF shallower than most cells, work toward overcoming this challenge is ongoing.

In the coming decade we envision SXT will be available at most synchrotron facilities. In addition, there has been much progress in the development of "tabletop" sources for SXT (Legall et al. 2012). These compact x-ray sources have improved enormously in terms of soft x-ray flux. This remains a very active research area,

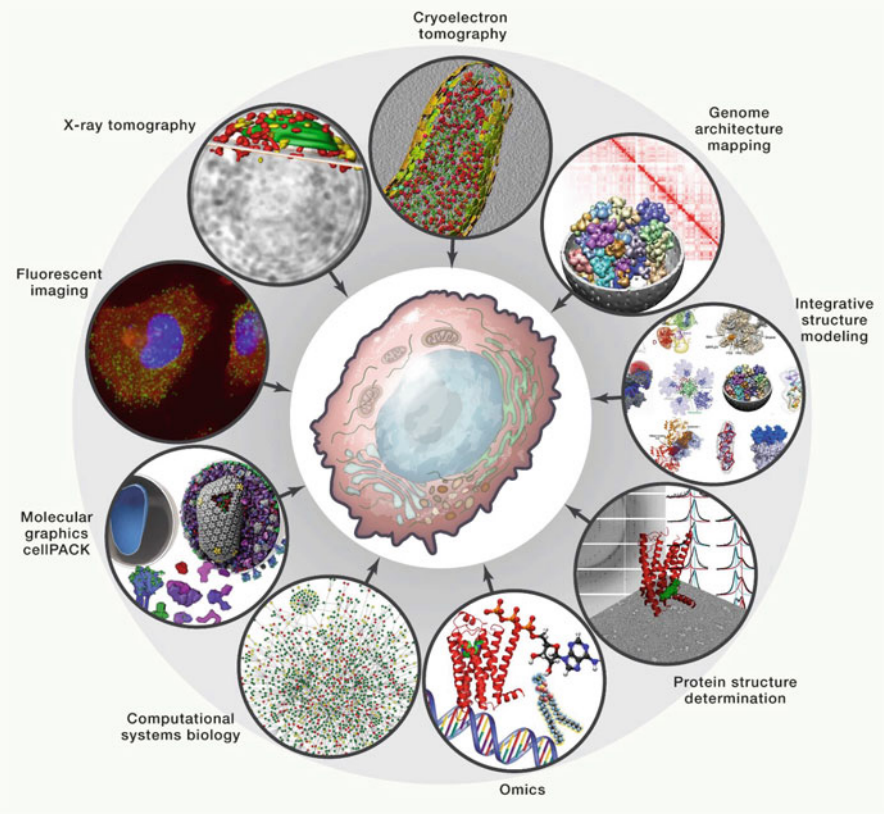

Fig. 13 The array of methods and disparate data types needed to build models of human pancreatic β cells that range in scale from atomic to cellular level. Fluorescent imaging (super-resolution imaging, live cell imaging), x-ray tomography, cryo-electron tomography, genome architecture mapping (Hi-C maps, fluorescent in situ hybridization, etc.), integrative structure modeling, protein structure determination (x-ray crystallography, electron microscopy, nuclear magnetic resonance spectroscopy), -omics (proteomics, transcriptomics, metabolomics, genomics, lipidomics), computational systems biology, and molecular graphics and packing tools. (Image taken from Singla et al. 2018)

with the promise that SXT could soon translate into technology well accessible to a laboratory or clinic.

Finally, correlated CFT-SXT has matured beyond the proof of concept stage (McDermott et al. 2009, 2012a, b; Schellenberger et al. 2014; Hagen et al. 2012; Cinquin et al. 2014; Duke et al. 2014; Hagen et al. 2014; Smith et al. 2013, 2014a, b; Zeev-Ben-Mordehai et al. 2014). The ability to localize molecules in the context of a high-resolution 3D reconstruction has captured the imagination of the cell biology community, making this combination of modalities a technique in high demand. The high-numerical aperture cryogenic light microscope used in proof of principle experiments by Larabell and colleagues was a low-budget instrument; while capable

of generating isotropic localization data, it was limited to a spatial resolution of several hundred nanometers. Consequently, this group (and presumably others) is now building next-generation high-numerical aperture cryogenic microscopes. This new instrument will be capable of combining tomographic methods with "super-resolution" techniques such as structured illumination microscopy (SIM) (Gustafsson 2000; Gustafsson et al. 2008; Schermelleh et al. 2008). The net output will be molecular localization information with very high, isotropic precision. The combination of this type of light microscopy with SXT is immensely powerful and capable of revealing if co-localization occurs within a single voxel in the reconstruction.

Modeling cells from the atomic to cellular scales remains a major challenge in biology and medicine. In this regard, CFT-SXT can play a significant role, by contributing to community-wide collaborations, such as the one dedicated to modeling human pancreatic β cells, as shown in Fig. 13.

Acknowledgments This work was supported by the US Department of Energy, Office of Biological and Environmental Research (DE-AC02-05CH11231), the National Center for Research Resources of the National Institutes of Health (P41RR019664) and the National Institutes of General Medicine of the National Institutes of Health (P41GM103445), the Gordon and Betty Moore Foundation, and the Chan Zuckerberg Initiative. V.W. is supported by a German Research Foundation research fellowship WE 6221/1-1.

References

Ö. Çiçek, A. Abdulkadir, S.S. Lienkamp, T. Brox, O. Ronneberger, 3D u-net: learning dense volumetric segmentation from sparse annotation, in *Medical Image Computing and Computer-Assisted Intervention – MICCAI 2016*, ed. by S. Ourselin, L. Joskowicz, M.R. Sabuncu, G. Unal, W. Wells (Springer International Publishing, Cham, 2016), pp. 424–432. ISBN 978-3-319-46723-8

J.-I. Agulleiro, J.-J. Fernandez, Tomo3D 2.0 – exploitation of advanced vector eXtensions (AVX) for 3D reconstruction. J. Struct. Biol. **189**(2), 147–152 (2015). https://doi.org/10.1016/j.jsb.2014.11.009

D. Attwood, *Soft X-Rays and Extreme Ultraviolet Radiation: Principles and Applications* (Cambridge University Press, Cambridge, 2007)

D. Attwood, W. Chao, E. Anderson, J.A. Liddle, B. Harteneck, P. Fischer, G. Schneider, M. Le Gros, C. Larabell, Imaging at high spatial resolution: soft x-ray microscopy to 15 nm. J. Biomed. Nanotechnol. **2**(2), 75–78 (2006). ISSN 1550–7033. https://doi.org/10.1166/jbn.2006.011.

K.V. Baev, K.A. Greene, F.F. Marciano, J.E. Samanta, A.G. Shetter, K.A. Smith, M.A. Stacy, R.F. Spetzler, Physiology and pathophysiology of cortico-basal ganglia-thalamocortical loops: theoretical and practical aspects. Prog. Neuro-Psychopharmacol. Biol. Psychiatry **26**(4), 771–804 (2002). ISSN 0278–5846. https://doi.org/10.1016/S0278-5846(02)00201-4

M. Beister, D. Kolditz, W.A. Kalender, Iterative reconstruction methods in x-ray CT. Phys. Med. **28**(2), 94–108 (2012)

M. Berglund, L. Rymell, M. Peuker, T. Wilhein, H.M. Hertz, Compact water-window transmission x-ray microscopy. J. Microsc. **197**(3), 268–273 (2000). https://doi.org/10.1046/j.1365-2818.2000.00675.x

M. Bertilson, O. von Hofsten, U. Vogt, A. Holmberg, H.M. Hertz, High-resolution computed tomography with a compact soft x-ray microscope. Opt. Express **17**(13), 11057–11065 (2009). https://doi.org/10.1364/OE.17.011057

M. Bertilson, O. von Hofsten, H.M. Hertz, U. Vogt, Numerical model for tomographic image formation in transmission x-ray microscopy. Opt. Express **19**(12), 11578–11583 (2011a)

M. Bertilson, O. von Hofsten, U. Vogt, A. Holmberg, A.E. Christakou, H.M. Hertz, Laboratory soft-x-ray microscope for cryotomography of biological specimens. Opt. Express **36**(14), 2728 (2011b). https://doi.org/10.1364/ol.36.002728

R. Bracewell, Strip integration in radio astronomy. Aust. J. Phys. **9**(2), 198 (1956). https://doi.org/10.1071/ph560198

D.B. Carlson, J. Gelb, V. Palshin, J.E. Evans, Laboratory-based cryogenic soft x-ray tomography with correlative cryo-light and electron microscopy. Microsc. Microanal. **19**(1), 22–29 (2013). https://doi.org/10.1017/s1431927612013827

R. Carzaniga, M.-C. Domart, L.M. Collinson, E. Duke, Cryo-soft x-ray tomography: a journey into the world of the native-state cell. Protoplasma **251**(2), 449–458 (2014). https://doi.org/10.1007/s00709-013-0583-y

J.-H. Chang, J.M. Anderson, J.R. Votaw, Regularized image reconstruction algorithms for positron emission tomography. IEEE Trans. Med. Imaging **23**(9), 1165–1175 (2004)

W. Chao, B.D. Harteneck, J.A. Liddle, E.H. Anderson, D.T. Attwood, Soft x-ray microscopy at a spatial resolution better than 15 nm. Nature **435**(7046), 1210–1213 (2005). https://doi.org/10.1038/nature03719

W. Chao, J. Kim, S. Rekawa, P. Fischer, E.H. Anderson, Demonstration of 12 nm resolution Fresnel zone plate lens based soft x-ray microscopy. Opt. Express **17**(20), 17669 (2009). https://doi.org/10.1364/oe.17.017669

H.N. Chapman, A. Barty, M.J. Bogan, S. Boutet, M. Frank, S.P. Hau-Riege, S. Marchesini, B.W. Woods, S. Bajt, W.H. Benner, R.A. London, E. Plönjes, M. Kuhlmann, R. Treusch, S. Düsterer, T. Tschentscher, J.R. Schneider, E. Spiller, T. Möller, C. Bostedt, M. Hoener, D.A. Shapiro, K.O. Hodgson, D. van der Spoel, F. Burmeister, M. Bergh, C. Caleman, G. Huldt, M.M. Seibert, F.R.N.C. Maia, R.W. Lee, A. Szöke, N. Timneanu, J. Hajdu, Femtosecond diffractive imaging with a soft-x-ray free-electron laser. Nat. Phys. **2**(12), 839–843 (2006). https://doi.org/10.1038/nphys461

B.P. Cinquin, M. Do, G. McDermott, A.D. Walters, M. Myllys, E.A. Smith, O. Cohen-Fix, M.A. Le Gros, C.A. Larabell, Putting molecules in their place. Eur. J. Cell Biol. **115**(2), 209–216 (2014)

F. Ciompi, B. de Hoop, S.J. van Riel, K. Chung, E.T. Scholten, M. Oudkerk, P.A. de Jong, M. Prokop, B. van Ginneken, Automatic classification of pulmonary peri-fissural nodules in computed tomography using an ensemble of 2D views and a convolutional neural network out-of-the-box. Med. Image Anal. **26**(1), 195–202 (2015)

E.J. Clowney, M.A. LeGros, C.P. Mosley, F.G. Clowney, E.C. Markenskoff-Papadimitriou, M. Myllys, G. Barnea, C.A. Larabell, S. Lomvardas, Nuclear aggregation of olfactory receptor genes governs their monogenic expression. Cell **151**(4), 724–737 (2012)

M. Cyrklaff, A. Linaroudis, M. Boicu, P. Chlanda, W. Baumeister, G. Griffiths, J. Krijnse-Locker, Whole cell cryo-electron tomography reveals distinct disassembly intermediates of vaccinia virus. PLoS One **2**(5), e420 (2007)

R. Dahl, L.A. Staehelin, High-pressure freezing for the preservation of biological structure: theory and practice. Microsc. Res. Tech. **13**(3), 165–174 (1989)

M.C. Darrow, Y. Zhang, B.P. Cinquin, E.A. Smith, R. Boudreau, R.H. Rochat, M.F. Schmid, Y. Xia, C.A. Larabell, W. Chiu, Visualizing red blood cell sickling and the effects of inhibition of sphingosine kinase 1 using soft x-ray tomography. J. Cell Sci. **129**(18), 3511–3517 (2016). https://doi.org/10.1242/jcs.189225

A.P. Dempster, N.M. Laird, D.B. Rubin, Maximum likelihood from incomplete data via the EM algorithm. J. R. Stat. Soc. Ser. B Methodol. **39**(1), 1–38 (1977)

G. Denbeaux, E. Anderson, W. Chao, T. Eimüller, L. Johnson, M. Köhler, C. Larabell, M. Legros, P. Fischer, A. Pearson, et al. Soft x-ray microscopy to 25 nm with applications to biology and magnetic materials. Nucl. Instrum. Methods Phys. Res. A **467**, 841–844 (2001)

G. Denbeaux, G. Schneider, A. Pearson, W. Chao, B. Bates, B. Harteneck, D. Olynick, E. Anderson, P. Fischer, M. Juenger, Recent progress with high resolution x-ray microscopy at the xm-1, in Journal de Physique IV (Proceedings), vol. 104 (EDP Sciences, 2003), pp. 9–9

B.A. Dowd, G.H. Campbell, R.B. Marr, V.V. Nagarkar, S.V. Tipnis, L. Axe, D.P. Siddons, Developments in synchrotron x-ray computed microtomography at the national synchrotron light source, in *Developments in X-ray Tomography II*, vol. 3772. International Society for Optics and Photonics (SPIE, Bellingham, 1999), pp. 224–237

J. Dubochet, M. Adrian, J.-J. Chang, J.-C. Homo, J. Lepault, A.W. McDowall, P. Schultz, Cryo-electron microscopy of vitrified specimens. Q. Rev. Biophys. **21**(2), 129–228 (1988)

E.M. Duke, M. Razi, A. Weston, P. Guttmann, S. Werner, K. Henzler, G. Schneider, S.A. Tooze, L.M. Collinson, Imaging endosomes and autophagosomes in whole mammalian cells using correlative cryo-fluorescence and cryo-soft x-ray microscopy (cryo-CLXM). Ultramicroscopy **143**, 77–87 (2014). https://doi.org/10.1016/j.ultramic.2013.10.006

A. Ekman, V. Weinhardt, J.-H. Chen, G. McDermott, M.A. Le Gros, C. Larabell, PSF correction in soft x-ray tomography. J. Struct. Biol. **204**, 9–18 (2018)

M.H. Ellisman, T.J. Deerinck, X. Shu, G.E. Sosinsky, Picking faces out of a crowd: genetic labels for identification of proteins in correlated light and electron microscopy imaging, in *Correlative Light and Electron Microscopy*, ed. by T. Müller-Reichert, P. Verkade. Methods in Cell Biology, vol. 111 (Elsevier, 2012), pp. 139–155. https://doi.org/10.1016/B978-0-12-416026-2.00008-X

R. Falcone, C. Jacobsen, J. Kirz, S. Marchesini, D. Shapiro, J. Spence, New directions in x-ray microscopy. Contemp. Phys. **52**(4), 293–318 (2011). https://doi.org/10.1080/00107514.2011.589662

J.A. Fessler, Aspire 3.0 user's guide: a sparse iterative reconstruction library. Technical report, Technical Report 293, Communications and Signal Processing Laboratory, Department of EECS, University of Michigan, Ann Arbor (1995)

J.A. Fessler, Mean and variance of implicitly defined biased estimators (such as penalized maximum likelihood): applications to tomography. IEEE Trans. Image Process. **5**(3), 493–506 (1996)

E. Fogelqvist, M. Kördel, V. Carannante, B. Önfelt, H.M. Hertz, Laboratory cryo x-ray microscopy for 3D cell imaging. Sci. Rep. **7**(1), 13433 (2017)

D. Gürsoy, F. De Carlo, X. Xiao, C. Jacobsen, Tomopy: a framework for the analysis of synchrotron tomographic data. J. Synchrotron Radiat. **21**(5), 1188–1193 (2014)

B.N.G. Giepmans, The fluorescent toolbox for assessing protein location and function. Science **312**(5771), 217–224 (2006). https://doi.org/10.1126/science.1124618

B.N. Giepmans, T.J. Deerinck, B.L. Smarr, Y.Z. Jones, M.H. Ellisman, Correlated light and electron microscopic imaging of multiple endogenous proteins using quantum dots. Nat. Methods **2**(10), 743 (2005)

P. Gilbert, Iterative methods for the three-dimensional reconstruction of an object from projections. J. Theor. Biol. **36**(1), 105–117 (1972). https://doi.org/10.1016/0022-5193(72)90180-4

B.M. Good, A.I. Su, Crowdsourcing for bioinformatics. Bioinformatics **29**(16), 1925–1933 (2013)

M.L. Gros, C. Knoechel, M. Uchida, D. Parkinson, G. McDermott, C. Larabell, 2.6 visualizing sub-cellular organization using soft x-ray tomography, in *Comprehensive Biophysics*, ed. by E.H. Egelman (Elsevier, Amsterdam, 2012), pp. 90–110. ISBN 978-0-08-095718-0. https://doi.org/10.1016/B978-0-12-374920-8.00212-5

L. Guo, Y. Guan, C. Wei, Y. Hu, Y. Tian, G. Liu, The study of radiation damage of yeast cells in cryo-soft x-ray tomography, in *Selected Papers of the Chinese Society for Optical Engineering Conferences held October and November 2016*, vol. 10255 (International Society for Optics and Photonics, 2017), p. 102551Q

M.G.L. Gustafsson, Surpassing the lateral resolution limit by a factor of two using structured illumination microscopy. SHORT COMMUNICATION. J. Microsc. **198**(2), 82–87 (2000). https://doi.org/10.1046/j.1365-2818.2000.00710.x

M.G. Gustafsson, L. Shao, P.M. Carlton, C.J.R. Wang, I.N. Golubovskaya, W.Z. Cande, D.A. Agard, J.W. Sedat, Three-dimensional resolution doubling in wide-field fluorescence

microscopy by structured illumination. Biophys. J. **94**(12), 4957–4970 (2008). https://doi.org/10.1529/biophysj.107.120345

W. Haddad, I. McNulty, J.E. Trebes, E. Anderson, et al., Ultrahigh-resolution x-ray tomography. Science **266**(5188), 1213 (1994)

N. Hafi, M. Grunwald, L.S. Van Den Heuvel, T. Aspelmeier, J.-H. Chen, M. Zagrebelsky, O.M. Schütte, C. Steinem, M. Korte, A. Munk, et al., Fluorescence nanoscopy by polarization modulation and polarization angle narrowing. Nat. Methods **11**(5), 579 (2014)

C. Hagen, P. Guttmann, B. Klupp, S. Werner, S. Rehbein, T.C. Mettenleiter, G. Schneider, K. Grünewald, Correlative VIS-fluorescence and soft x-ray cryo-microscopy/tomography of adherent cells. J. Struct. Biol. **177**(2), 193–201 (2012). https://doi.org/10.1016/j.jsb.2011.12.012

C. Hagen, S. Werner, S. Carregal-Romero, A.N. Malhas, B.G. Klupp, P. Guttmann, S. Rehbein, K. Henzler, T.C. Mettenleiter, D.J. Vaux, et al., Multimodal nanoparticles as alignment and correlation markers in fluorescence/soft x-ray cryo-microscopy/tomography of nucleoplasmic reticulum and apoptosis in mammalian cells. Ultramicroscopy **146**, 46–54 (2014)

E. Hanssen, C. Knoechel, M. Dearnley, M.W. Dixon, M.L. Gros, C. Larabell, L. Tilley, Soft x-ray microscopy analysis of cell volume and hemoglobin content in erythrocytes infected with asexual and sexual stages of Plasmodium falciparum. J. Struct. Biol. **177**(2), 224–232 (2012). https://doi.org/10.1016/j.jsb.2011.09.003

M. Harkiolaki, M.C. Darrow, M.C. Spink, E. Kosior, K. Dent, E. Duke, Cryo-soft x-ray tomography: using soft x-rays to explore the ultrastructure of whole cells. Emerg. Top. Life Sci. **2**(1), 81–92 (2018)

B. Henke, E. Gullikson, J. Davis, X-Ray interactions: photoabsorption, scattering, transmission, and reflection at E = 50–30,000 eV, Z = 1–92. At. Data Nucl. Data Tables **54**(2), 181–342 (1993). https://doi.org/10.1006/adnd.1993.1013

H. Hertz, O. von Hofsten, M. Bertilson, U. Vogt, A. Holmberg, J. Reinspach, D. Martz, M. Selin, A. Christakou, J. Jerlström-Hultqvist et al., Laboratory cryo soft x-ray microscopy. J. Struct. Biol. **177**(2), 267–272 (2012)

J.B. Heymann, D.M. Belnap, Bsoft: image processing and molecular modeling for electron microscopy. J. Struct. Biol. **157**(1), 3–18 (2007). https://doi.org/10.1016/j.jsb.2006.06.006

M. Holler, A. Diaz, M. Guizar-Sicairos, P. Karvinen, E. Färm, E. Härkönen, M. Ritala, A. Menzel, J. Raabe, O. Bunk, X-ray ptychographic computed tomography at 16 nm isotropic 3D resolution. Sci. Rep. **4**, 3857 (2014)

H.H. Hopkins, On the diffraction theory of optical images. Proc. R. Soc. A Math. Phys. Eng. Sci. **217**(1130), 408–432 (1953). https://doi.org/10.1098/rspa.1953.0071

S.F. Horne, J. Silterra, W. Holber, A compact soft x-ray microscope using an electrode-less Z-pinch source. J. Phys. Conf. Ser. **186**(1), 012028 (2009). http://stacks.iop.org/1742-6596/186/i=1/a=012028

B. Huang, Super-resolution optical microscopy: multiple choices. Curr. Opin. Chem. Biol. **14**(1), 10–14 (2010)

X. Huang, J. Nelson, J. Kirz, E. Lima, S. Marchesini, H. Miao, A.M. Neiman, D. Shapiro, J. Steinbrener, A. Stewart, et al., Soft x-ray diffraction microscopy of a frozen hydrated yeast cell. Phys. Rev. Lett. **103**(19):198101 (2009)

L. Jochum, W. Meyer-Ilse, Partially coherent image formation with x-ray microscopes. Appl. Opt. **34**(22), 4944 (1995). https://doi.org/10.1364/ao.34.004944

R. Kaufmann, C. Hagen, K. Grünewald, Fluorescence cryo-microscopy: current challenges and prospects. Curr. Opin. Chem. Biol. **20**, 86–91 (2014a)

R. Kaufmann, P. Schellenberger, E. Seiradake, I.M. Dobbie, E.Y. Jones, I. Davis, C. Hagen, K. Grünewald, Super-resolution microscopy using standard fluorescent proteins in intact cells under cryo-conditions. Nano Lett. **14**(7), 4171–4175 (2014b)

K.-J. Kim, Characteristics of synchrotron radiation, in *AIP Conference Proceedings* (AIP Publishing, 1989). https://doi.org/10.1063/1.38046

K.W. Kim, Y. Kwon, K.-Y. Nam, J.-H. Lim, K.-G. Kim, K.S. Chon, B.H. Kim, D.E. Kim, J. Kim, B.N. Ahn, H.J. Shin, S. Rah, K.-H. Kim, J.S. Chae, D.G. Gweon, D.W. Kang, S.H. Kang,

J.Y. Min, K.-S. Choi, S.E. Yoon, E.-A. Kim, Y. Namba, K.-H. Yoon, Compact soft x-ray transmission microscopy with sub-50 nm spatial resolution. Phys. Med. Biol. **51**(6), N99–N107 (2006). https://doi.org/10.1088/0031-9155/51/6/n01

J. Kirz, C. Jacobsen, M. Howells, Soft x-ray microscopes and their biological applications. Q. Rev. Biophys. **28**(1), 33–130 (1995)

J. Klukowska, G.T. Herman, J. Otón, R. Marabini, J.-M. Carazo, The soft x-ray transform. Inverse Prob. **30**(12), 125015 (2014). https://doi.org/10.1088/0266-5611/30/12/125015

C. Knöchel, *Anwendung und Anpassung tomographischer Verfahren in der Röntgenmikroskopie* (Logos-Verlag, Berlin, 2005)

B.G. Kopek, G. Shtengel, C.S. Xu, D.A. Clayton, H.F. Hess, Correlative 3D superresolution fluorescence and electron microscopy reveal the relationship of mitochondrial nucleoids to membranes. Proc. Natl. Acad. Sci. **109**(16), 6136–6141 (2012)

J.R. Kremer, D.N. Mastronarde, J.R. McIntosh, Computer visualization of three-dimensional image data using IMOD. J. Struct. Biol. **116**(1), 71–76 (1996)

W. Kukulski, M. Schorb, S. Welsch, A. Picco, M. Kaksonen, J.A. Briggs, Correlated fluorescence and 3d electron microscopy with high sensitivity and spatial precision. J. Cell Biol. **192**(1), 111–119 (2011)

C.A. Larabell, M.A. Le Gros, X-ray tomography generates 3-D reconstructions of the yeast, *Saccharomyces cerevisiae*, at 60-nm resolution. Mol. Biol. Cell **15**(3), 957–962 (2004). https://doi.org/10.1091/mbc.e03-07-0522

C.A. Larabell, K.A. Nugent, Imaging cellular architecture with x-rays. Curr. Opin. Struct. Biol. **20**(5), 623–631 (2010). https://doi.org/10.1016/j.sbi.2010.08.008

H. Legall, G. Blobel, H. Stiel, W. Sandner, C. Seim, P. Takman, D.H. Martz, M. Selin, U. Vogt, H.M. Hertz, D. Esser, H. Sipma, J. Luttmann, M. Höfer, H.D. Hoffmann, S. Yulin, T. Feigl, S. Rehbein, P. Guttmann, G. Schneider, U. Wiesemann, M. Wirtz, W. Diete, Compact x-ray microscope for the water window based on a high brightness laser plasma source. Opt. Express **20**(16), 18362 (2012). https://doi.org/10.1364/oe.20.018362

A. Leis, B. Rockel, L. Andrees, W. Baumeister, Visualizing cells at the nanoscale. Trends Biochem. Sci. **34**(2), 60–70 (2009). https://doi.org/10.1016/j.tibs.2008.10.011

M. Le Gros, G. McDermott, M. Uchida, C. Knoechel, C. Larabell, High-aperture cryogenic light microscopy. J. Microsc. **235**(1), 1–8 (2009)

M.A. Le Gros, G. McDermott, B.P. Cinquin, E.A. Smith, M. Do, W.L. Chao, P.P. Naulleau, C.A. Larabell, Biological soft x-ray tomography on beamline 2.1 at the advanced light source. J. Synchrotron Radiat. **21**(6), 1370–1377 (2014)

M.A. Le Gros, E.J. Clowney, A. Magklara, A. Yen, E. Markenscoff-Papadimitriou, B. Colquitt, M. Myllys, M. Kellis, S. Lomvardas, C.A. Larabell, Soft x-ray tomography reveals gradual chromatin compaction and reorganization during neurogenesis in vivo. Cell Rep. **17**(8), 2125–2136 (2016)

F. Li, Y. Guan, Y. Xiong, X. Zhang, G. Liu, Y. Tian, Method for extending the depth of focus in x-ray microscopy. Opt. Express **25**(7), 7657–7667 (2017)

Y. Liu, J. Wang, Y. Hong, Z. Wang, K. Zhang, P.A. Williams, P. Zhu, J.C. Andrews, P. Pianetta, Z. Wu, Extended depth of focus for transmission x-ray microscope. Opt. Lett. **37**(17), 3708–3710 (2012). https://doi.org/10.1364/OL.37.003708

J. Liu, F. Li, L. Chen, Y. Guan, L. Tian, Y. Xiong, G. Liu, Y. Tian, Quantitative imaging of candida utilis and its organelles by soft x-ray Nano-CT. J. Microsc. **270**(1), 64–70 (2018a)

T.-L. Liu, S. Upadhyayula, D.E. Milkie, V. Singh, K. Wang, I.A. Swinburne, K.R. Mosaliganti, Z.M. Collins, T.W. Hiscock, J. Shea, A.Q. Kohrman, T.N. Medwig, D. Dambournet, R. Forster, B. Cunniff, Y. Ruan, H. Yashiro, S. Scholpp, E.M. Meyerowitz, D. Hockemeyer, D.G. Drubin, B.L. Martin, D. Q. Matus, M. Koyama, S.G. Megason, T. Kirchhausen, E. Betzig, Observing the cell in its native state: imaging subcellular dynamics in multicellular organisms. Science **360**(6386) (2018b). ISSN 0036-8075. https://doi.org/10.1126/science.aaq1392

V. Lučić, A.H. Kossel, T. Yang, T. Bonhoeffer, W. Baumeister, A. Sartori, Multiscale imaging of neurons grown in culture: from light microscopy to cryo-electron tomography. J. Struct. Biol. **160**(2), 146–156 (2007)

I. Luengo, M.C. Darrow, M.C. Spink, Y. Sun, W. Dai, C.Y. He, W. Chiu, T. Pridmore, A.W. Ashton, E.M. Duke, M. Basham, A.P. French, Survos: super-region volume segmentation workbench. J. Struct. Biol. **198**(1), 43–53 (2017). ISSN 1047-8477. https://doi.org/10.1016/j.jsb.2017.02.007

M.E. Martone, T.J. Deerinck, N. Yamada, E. Bushong, M.H. Ellisman, Correlated 3D light and electron microscopy: use of high voltage electron microscopy and electron tomography for imaging large biological structures. J. Histotechnol. **23**(3), 261–270 (2000)

G. McDermott, M.A.L. Gros, C.G. Knoechel, M. Uchida, C.A. Larabell, Soft x-ray tomography and cryogenic light microscopy: the cool combination in cellular imaging. Trends Cell Biol. **19**(11), 587–595 (2009). https://doi.org/10.1016/j.tcb.2009.08.005

G. McDermott, D.M. Fox, L. Epperly, M. Wetzler, A.E. Barron, M.A. Le Gros, C.A. Larabell, Visualizing and quantifying cell phenotype using soft x-ray tomography. Bioessays **34**(4), 320–327 (2012a)

G. McDermott, M.A. Le Gros, C.A. Larabell, Visualizing cell architecture and molecular location using soft x-ray tomography and correlated cryo-light microscopy. Annu. Rev. Phys. Chem. **63**, 225–239 (2012b)

S.G. Megason, S.E. Fraser, Imaging in systems biology. Cell **130**(5), 784–795 (2007)

J. Miao, K.O. Hodgson, T. Ishikawa, C.A. Larabell, M.A. LeGros, Y. Nishino, Imaging whole *Escherichia coli* bacteria by using single-particle x-ray diffraction. Proc. Natl. Acad. Sci. **100**(1), 110–112 (2003)

A.G. Michette, I.C.E. Turcu, M.S. Schulz, M.T. Browne, G.R. Morrison, P. Fluck, C.J. Buckley, G.F. Foster, Scanning x-ray microscopy using a laser-plasma source. Rev. Sci. Instrum. **64**(6), 1478 (1993). https://doi.org/10.1063/1.1144067

A. Mirone, E. Brun, E. Gouillart, P. Tafforeau, J. Kieffer, The pyhst2 hybrid distributed code for high speed tomographic reconstruction with iterative reconstruction and a priori knowledge capabilities. Nucl. Instrum. Methods Phys. Res. B **324**, 41–48 (2014)

M. Myllys, V. Ruokolainen, V. Aho, E.A. Smith, S. Hakanen, P. Peri, A. Salvetti, J. Timonen, V. Hukkanen, C.A. Larabell, et al., Herpes simplex virus 1 induces egress channels through marginalized host chromatin. Sci. Rep. **6**, 28844 (2016)

F. Natterer, *Computerized Tomography* (Vieweg+Teubner Verlag, Wiesbaden, 1986), pp. 1–8. ISBN 978-3-663-01409-6. https://doi.org/10.1007/978-3-663-01409-6_1

J. Otón, C. Sorzano, E. Pereiro, J. Cuenca-Alba, R. Navarro, J.M. Carazo, R. Marabini, Image formation in cellular x-ray microscopy. J. Struct. Biol. **178**(1), 29–37 (2012). https://doi.org/10.1016/j.jsb.2012.01.006

J. Otón, E. Pereiro, J.J. Conesa, F.J. Chichón, D. Luque, J.M. Rodríguez, A.J. Pérez-Berná, C.O.S. Sorzano, J. Klukowska, G.T. Herman, et al., Xtend: extending the depth of field in cryo soft x-ray tomography. Sci. Rep. **7**, 45808 (2017). https://doi.org/10.1038/srep45808

D.Y. Parkinson, C. Knoechel, C. Yang, C.A. Larabell, M.A. Le Gros, Automatic alignment and reconstruction of images for soft x-ray tomography. J. Struct. Biol. **177**(2), 259–266 (2012)

D.Y. Parkinson, L.R. Epperly, G. McDermott, M.A. Le Gros, R.M. Boudreau, C.A. Larabell, Nanoimaging cells using soft x-ray tomography, in *Nanoimaging: Methods and Protocols*, ed. by A.A. Sousa (Humana Press, Totowa, 2013), pp. 457–481. https://doi.org/10.1007/978-1-62703-137-0_25

D.M. Pelt, J.A. Sethian, A mixed-scale dense convolutional neural network for image analysis. Proc. Natl. Acad. Sci. **115**(2), 254–259 (2018). https://doi.org/10.1073/pnas.1715832114

E. Pereiro, J. Nicolás, S. Ferrer, M.R. Howells, A soft x-ray beamline for transmission x-ray microscopy at ALBA. J. Synchrotron Radiat. **16**(4), 505–512 (2009). https://doi.org/10.1107/s0909049509019396

J. Radon, On determination of functions by their integral values along certain multiplicities. Berichte der Sächische Akademie der Wissenschaften Leipzig, (Germany) **69**, 262–277 (1917)

S. Rehbein, S. Heim, P. Guttmann, S. Werner, G. Schneider, Ultrahigh-resolution soft-x-ray microscopy with zone plates in high orders of diffraction. Phys. Rev. Lett. **103**(11), 110801 (2009)

H.R. Roth, L. Lu, A. Seff, K.M. Cherry, J. Hoffman, S. Wang, J. Liu, E. Turkbey, R.M. Summers, A new 2.5 D representation for lymph node detection using random sets of deep convolutional

neural network observations, in *International Conference on Medical Image Computing and Computer-Assisted Intervention* (Springer, 2014), pp. 520–527

M.S. Roth, S.J. Cokus, S.D. Gallaher, A. Walter, D. Lopez, E. Erickson, B. Endelman, D. Westcott, C.A. Larabell, S.S. Merchant, et al., Chromosome-level genome assembly and transcriptome of the green alga *Chromochloris zofingiensis* illuminates astaxanthin production. Proc. Natl. Acad. Sci. **114**(21), E4296–E4305 (2017)

L. Rymell, H. Hertz, Droplet target for low-debris laser-plasma soft x-ray generation. Opt. Commun. **103**(1–2), 105–110 (1993). https://doi.org/10.1016/0030-4018(93)90651-k

P. Schellenberger, R. Kaufmann, C.A. Siebert, C. Hagen, H. Wodrich, K. Grünewald, High-precision correlative fluorescence and electron cryo microscopy using two independent alignment markers. Ultramicroscopy **143**, 41–51 (2014)

L. Schermelleh, P.M. Carlton, S. Haase, L. Shao, L. Winoto, P. Kner, B. Burke, M.C. Cardoso, D.A. Agard, M.G.L. Gustafsson, H. Leonhardt, J.W. Sedat, Subdiffraction multicolor imaging of the nuclear periphery with 3D structured illumination microscopy. Science **320**(5881), 1332–1336 (2008). https://doi.org/10.1126/science.1156947

G. Schneider, G. Denbeaux, E. Anderson, A. Pearson, W. Bates, S. Vogt, C. Knochen, M.A. Meyer, E. Zschech, High resolution x-ray tomography with applications in biology and materials science. J. Phys. IV **104**, 607–613 (2003). https://doi.org/10.1051/jp4:20030155

G. Schneider, P. Guttmann, S. Heim, S. Rehbein, F. Mueller, K. Nagashima, J.B. Heymann, W.G. Müller, J.G. McNally, Three-dimensional cellular ultrastructure resolved by x-ray microscopy. Nat. Methods **7**(12), 985–987 (2010). https://doi.org/10.1038/nmeth.1533

G. Schneider, P. Guttmann, S. Rehbein, S. Werner, R. Follath, Cryo x-ray microscope with flat sample geometry for correlative fluorescence and nanoscale tomographic imaging. J. Struct. Biol. **177**(2), 212–223 (2012). https://doi.org/10.1016/j.jsb.2011.12.023

M. Selin, E. Fogelqvist, A. Holmberg, P. Guttmann, U. Vogt, H.M. Hertz, 3D simulation of the image formation in soft x-ray microscopes. Opt. Express **22**(25), 30756–30768 (2014)

M. Selin, E. Fogelqvist, S. Werner, H.M. Hertz, Tomographic reconstruction in soft x-ray microscopy using focus-stack back-projection. Opt. Lett. **40**(10), 2201–2204 (2015)

D. Shapiro, P. Thibault, T. Beetz, V. Elser, M. Howells, C. Jacobsen, J. Kirz, E. Lima, H. Miao, A.M. Neiman, D. Sayre, Biological imaging by soft x-ray diffraction microscopy. Proc. Natl. Acad. Sci. **102**(43), 15343–15346 (2005). https://doi.org/10.1073/pnas.0503305102

C.J.R. Sheppard, Defocused transfer function for a partially coherent microscope and application to phase retrieval. J. Opt. Soc. Am. A **21**(5), 828–831 (2004). https://doi.org/10.1364/JOSAA.21.000828

C. Sheppard, X. Mao, Three-dimensional imaging in a microscope. JOSA A **6**(9), 1260–1269 (1989)

A. Shkolyar, A. Gefen, D. Benayahu, H. Greenspan, Automatic detection of cell divisions (mitosis) in live-imaging microscopy images using convolutional neural networks, in *2015 37th Annual International Conference of the IEEE Engineering in Medicine and Biology Society (EMBC)*. IEEE, pp. 743–746 (2015)

J. Singla, K.M. McClary, K.L. White, F. Alber, A. Sali, R.C. Stevens, Opportunities and challenges in building a spatiotemporal multi-scale model of the human pancreatic β cell. Cell **173**(1), 11–19 (2018)

M. Slaney, A.C. Kak, L.E. Larsen, Limitations of imaging with first-order diffraction tomography. IEEE Trans. Microwave Theory Tech. **32**(8), 860–874 (1984)

E.A. Smith, B.P. Cinquin, G. McDermott, M.A. Le Gros, D.Y. Parkinson, H.T. Kim, C.A. Larabell, Correlative microscopy methods that maximize specimen fidelity and data completeness, and improve molecular localization capabilities. J. Struct. Biol. **184**(1), 12–20 (2013)

E.A. Smith, B.P. Cinquin, M. Do, G. McDermott, M.A. Le Gros, C.A. Larabell, Correlative cryogenic tomography of cells using light and soft x-rays. Ultramicroscopy **143**, 33–40 (2014a)

E.A. Smith, G. McDermott, M. Do, K. Leung, B. Panning, M.A. Le Gros, C.A. Larabell, Quantitatively imaging chromosomes by correlated cryo-fluorescence and soft x-ray tomographies. Biophys. J. **107**(8), 1988–1996 (2014b)

A. Sorrentino, J. Nicolás, R. Valcárcel, F.J. Chichón, M. Rosanes, J. Avila, A. Tkachuk, J. Irwin, S. Ferrer, E. Pereiro, MISTRAL: a transmission soft x-ray microscopy beamline for cryo nano-tomography of biological samples and magnetic domains imaging. J. Synchrotron Radiat. **22**(4), 1112–1117 (2015). https://doi.org/10.1107/s1600577515008632

N. Streibl, Three-dimensional imaging by a microscope. J. Opt. Soc. Am. A **2**(2), 121 (1985). https://doi.org/10.1364/josaa.2.000121

Y.-J. Su, H.-W. Fu, S.-C. Chung, H.-S. Fung, D.-G. Liu, L.-J. Huang, H.-Y. Yan, Y.-C. Chou, G.-C. Yin, L.-J. Lai, Design of the soft x-ray tomography beamline at Taiwan photon source, in *Proceedings of the 12th International Conference on Synchrotron Radiation Instrumentation*. (AIP Publishing, 2016). https://doi.org/10.1063/1.4952869

S. Subramaniam, Bridging the imaging gap: visualizing subcellular architecture with electron tomography. Curr. Opin. Microbiol. **8**(3), 316–322 (2005)

S. Trattner, M. Feigin, H. Greenspan, N. Sochen, Validity criterion for the born approximation convergence in microscopy imaging. JOSA A **26**(5), 1147–1156 (2009)

R.Y. Tsien, Building and breeding molecules to spy on cells and tumors. FEBS Lett. **579**(4), 927–32 (2005)

M. Uchida, Y. Sun, G. McDermott, C. Knoechel, M.A. Le Gros, D. Parkinson, D.G. Drubin, C.A. Larabell, Quantitative analysis of yeast internal architecture using soft x-ray tomography. Yeast **28**(3), 227–236 (2011)

W. van Aarle, W.J. Palenstijn, J. Cant, E. Janssens, F. Bleichrodt, A. Dabravolski, J. De Beenhouwer, K.J. Batenburg, J. Sijbers, Fast and flexible x-ray tomography using the astra toolbox. Opt. Express **24**(22), 25129–25147 (2016)

C. Van Rijnsoever, V. Oorschot, J. Klumperman, Correlative light-electron microscopy (CLEM) combining live-cell imaging and immunolabeling of ultrathin cryosections. Nat. Methods **5**(11), 973 (2008)

N. Varsano, T. Dadosh, S. Kapishnikov, E. Pereiro, E. Shimoni, X. Jin, H.S. Kruth, L. Leiserowitz, L. Addadi, Development of correlative cryo-soft x-ray tomography and stochastic reconstruction microscopy. A study of cholesterol crystal early formation in cells. J. Am. Chem. Soc. **138**(45), 14931–14940 (2016)

O. von Hofsten, P.A. Takman, U. Vogt, Simulation of partially coherent image formation in a compact soft x-ray microscope. Ultramicroscopy **107**(8), 604–609 (2007). https://doi.org/10.1016/j.ultramic.2006.12.001

D. Weiß, G. Schneider, B. Niemann, P. Guttmann, D. Rudolph, G. Schmahl, Computed tomography of cryogenic biological specimens based on x-ray microscopic images. Ultramicroscopy **84**(3–4), 185–197 (2000). ISSN 0304-3991. https://doi.org/10.1016/S0304-3991(00)00034-6

A. Weiner, S. Kapishnikov, E. Shimoni, S. Cordes, P. Guttmann, G. Schneider, M. Elbaum, Vitrification of thick samples for soft x-ray cryo-tomography by high pressure freezing. J. Struct. Biol. **181**(1), 77–81 (2013). ISSN 1047-8477. https://doi.org/10.1016/j.jsb.2012.10.005

T. Zeev-Ben-Mordehai, C. Hagen, K. Grünewald, A cool hybrid approach to the herpesvirus 'life' cycle. Curr. Opin. Virol. **5**, 42–49 (2014)

W. Zhang, R. Li, H. Deng, L. Wang, W. Lin, S. Ji, D. Shen, Deep convolutional neural networks for multi-modality isointense infant brain image segmentation. NeuroImage **108**, 214–224 (2015)